Title

Organization of the sleep-related neural systems in the brain of the minke whale (Balaenoptera acutorostrata)

Journal

The Journal of Comparative Neurology, 524(10)

ISSN

1550-7149

Authors

Dell, Leigh-Anne
Karlsson, Karl Ae
Patzke, Nina
et al.

Publication Date

2016-07-01

DOI

10.1002/cne.23931

Peer reviewed

Published in final edited form as:

J Comp Neurol. 2016 July 01; 524(10): 2018–2035. doi:10.1002/cne.23931.

Organization of the Sleep-Related Neural Systems in the Brain of the Minke Whale *(Balaenoptera acutorostrata)*

Leigh-Anne Dell[1], **Karl Æ. Karlsson**[2], **Nina Patzke**[1], **Muhammad A. Spocter**[1,3], **Jerome M. Siegel**[4], **Paul R. Manger**[1,*]

[1]School of Anatomical Sciences, Faculty of Health Sciences, University of the Witwatersrand, Johannesburg, Republic of South Africa

[2]Biomedical Engineering, Reykjavik University, Reykjavik, Iceland

[3]Department of Anatomy, Des Moines University, Des Moines, Iowa, USA

[4]Department of Psychiatry, University of California, Los Angeles, Neurobiology Research 151A3, Sepulveda VAMC, North Hills, California, USA

Abstract

The current study analyzed the nuclear organization of the neural systems related to the control and regulation of sleep and wake in the basal forebrain, diencephalon, midbrain, and pons of the minke whale, a mysticete cetacean. While odontocete cetaceans sleep in an unusual manner, with unihemispheric slow wave sleep (USWS) and suppressed REM sleep, it is unclear whether the mysticete whales show a similar sleep pattern. Previously, we detailed a range of features in the odontocete brain that appear to be related to odontocete-type sleep, and here present our analysis of these features in the minke whale brain. All neural elements involved in sleep regulation and control found in bihemispheric sleeping mammals and the harbor porpoise were present in the minke whale, with no specific nuclei being absent, and no novel nuclei being present. This qualitative similarity relates to the cholinergic, noradrenergic, serotonergic and orexinergic systems, and the GABAergic elements of these nuclei. Quantitative analysis revealed that the numbers of pontine cholinergic (274,242) and noradrenergic (203,686) neurons, and hypothalamic orexinergic neurons (277,604), are markedly higher than other large-brained bihemispheric sleeping mammals. Small telencephalic commissures (anterior, corpus callosum, and hippocampal), an enlarged posterior commissure, supernumerary pontine cholinergic and noradrenergic cells, and an enlarged peripheral division of the dorsal raphe nuclear complex of the minke whale, all indicate that the suite of neural characteristics thought to be involved in

*CORRESPONDENCE TO: Paul Manger, School of Anatomical Sciences, Faculty of Health Sciences, University of the Witwatersrand, 7 York Road, Parktown, 2193, Johannesburg, Republic of South Africa. Paul.Manger@wits.ac.za.

ROLE OF AUTHORS

LAD, KÆK, NP, MAS, JMS, and PRM conceptualized the study. KÆK and PRM obtained the brains, and LAD, NP, and PRM did the immunohistochemical staining and reconstructions. LAD and MAS undertook the quantitative and statistical analysis of the data. LAD and PRM wrote the article and the remaining authors contributed to the editing and improvement of the early drafts of the article. All authors had full access to all of the data in the study and take responsibility for the integrity of the data and the accuracy of the data analysis.

CONFLICT OF INTEREST

The authors declare no conflicts of interest.

the control of USWS and the suppression of REM in the odontocete cetaceans are present in the minke whale.

Keywords

Cetacea; Mysticete; Cetartiodactyla; mammalian sleep; unihemispheric sleep; brain evolution; RRID AB_2079751; RRID AB_10000323; RRID AB_91545; RRID AB_10000343; RRID AB_10000340; RRID AB_10000321

The minke whale, *Balaenoptera acutorostrata*, is a cetacean belonging to the suborder mysticete, and while being the smallest member of the baleen whales, can grow to about 10 meters in length and attain a body mass of about 9,000 kg (Eriksen and Pakkenberg, 2007). Minke whales are found throughout the North Atlantic ocean, but are more common in coastal or shelf areas (Horwood, 1990; Kot et al., 2012). In terms of understanding the potential for unihemispheric sleep in mysticetes, very little research has been undertaken and most inferences regarding the manner in which mysticete whales sleep are derived from studies on odontocetes (see Mukhametov et al., 1976, 1977; Lyamin et al., 2002, 2008). The only documented studies of sleep in a mysticete whale are those by Lyamin et al. (2000, 2001), where they examined resting behavior in a single gray whale calf. These studies concluded that mysticetes appear to have unihemispheric slow wave sleep (USWS), due to alternate eye openings and closing during the rest period, and that there may be a small amount of REM sleep, but that this would occur without hypotonia and is represented by single or multiple muscle jerks during the general resting period.

The only studies of the neural systems related to the sleep–wake cycle undertaken on the brains of mysticete whales to date were the observations that, as with odontocete cetaceans, the mysticete cetaceans appear to have a low-density orexinergic terminal network in the cerebral cortex (Dell et al., 2015) and an enlarged posterior commissure (Lyamin et al., 2008). In odontocete cetaceans, a small corpus callosum (Manger et al., 2010) and anterior commissure, coupled with a large posterior commissure, appear to provide supportive correlates to hemispheric independence during slow wave sleep (Lyamin et al., 2008; Dell et al., 2016). Despite this, the organization of the specific neurochemical systems involved in the regulation of the sleep–wake cycle in cetaceans does not appear to be qualitatively different from that found in other mammals (Manger et al., 2003; Lyamin et al., 2008; Dell et al., 2012, 2015, 2016), although quantitative differences are apparent (Dell et al., 2012, 2015, 2016).

In order to fill the gap in our knowledge regarding the neural basis of sleep in the mysticete whales, the current study examined the nuclear organization of the cholinergic, catecholaminergic, serotonergic, and orexinergic systems associated with sleep and wake in the minke whale. In addition, the distribution of the putative GABAergic neurons and terminal networks associated with the sleep/wake systems were examined by staining for the calcium-binding proteins parvalbumin, calbindin, and calretinin. Thus, we investigated the basal forebrain, diencephalon, and pons of the minke whale. Stereological analysis of neuronal numbers was undertaken for the laterodorsal tegmental nucleus (LDT) and pedunculopontine tegmental nucleus (PPT), as well as the locus coeruleus complex (LC)

and the orexinergic neurons of the hypothalamus. The aim of this study was to provide a clearer understanding of the neural basis of cetacean sleep regulation and control as well as to provide better insight into the function and evolution of cetacean sleep phenomenology from a mysticete whale's perspective.

MATERIALS AND METHODS

Specimens

Brains from six adult male northern minke whales (*Balaenoptera acutorostrata)* (brain masses ranged between 2.6–3.2 kg and body length ranged between 6.3–8.7 m) were acquired during the whaling season in Iceland in partnership the Iceland Ministry of Fisheries and Agriculture. The animals were treated and used according to the guidelines of the University of Witwatersrand Animal Ethics Committee, which correspond with those of the National Institutes of Health (NIH) for the care and use of animals in scientific experimentation. The animals were obtained after being sacrificed according to Icelandic commercial whaling practices. Once sacrificed, the heads of the animals were removed from the body and the brains removed from the skulls and immersion fixed in 4% paraformaldehyde in 0.1M phosphate buffer (PB) for 72 hours at 4°C. The brains were then transferred to a solution of 30% sucrose in 0.1M PB at 4°C until they had equilibrated (~14 days) and were then transferred to an antifreeze solution containing 30% glycerol, 30% ethylene glycol, 30% distilled water, and 10% 0.244M PB. Once again the brains were allowed to equilibrate (14 days) in the solution at 4°C and were then moved to the −20°C freezer for storage until sectioning.

Tissue selection and immunostaining

Prior to sectioning, all brains underwent magnetic resonance imaging (MRI) to reveal the general anatomy of the brain of the northern minke whale (see Manger et al., 2010, 2012; Maseko et al., 2011, 2012, for MRI protocol). As all specimens showed a similar anatomy (i.e., there was no obvious variance between the specimens), we selected a single specimen (BA1, brain mass 2,900 g) to section for subsequent staining. The basal forebrain, diencephalon, midbrain, and pons were dissected from the remainder of the brain as a single block of tissue. This block of tissue was placed in 30% sucrose in 0.1M PB at 4°C until it had equilibrated. The tissue was then frozen in crushed dry ice and mounted onto an aluminum stage that was attached to a freezing microtome modified to allow the sectioning of large tissue blocks. The entire tissue block was sectioned in the coronal plane, with a section thickness of 50 μm. A 1-in-20 series of sections was taken and nine series were stained for Nissl substance, myelin, choline acetyltransferase (ChAT), tyrosine hydroxylase (TH), serotonin (5HT), orexin (OxA), parvalbumin (PV), calbindin (CB), and calretinin (CR), while the remaining 11 series were placed back in antifreeze solution and returned to the freezer for future use. Sections used for Nissl, myelin, and immunohistochemical staining were treated as described in Dell et al. (2016). The only difference to this previous study was the inclusion of the orexinergic immunostaining. To reveal orexinergic neurons, anti-orexin-A (OxA) (AB3704, Merck-Millipore, Darmstadt, Germany, raised in rabbit) at a dilution of 1:3,000 was used. All sections were examined with a stereomicroscope and the architectonic borders of the sections were traced according to the Nissl and myelin-stained

sections using a camera lucida. The immunostained sections were then matched to the traced drawings, adjusted slightly for any differential shrinking of the stained sections, and immunopositive neurons were marked. The drawings were then scanned and redrawn using the Canvas 8 (Deneba, Miami, FL) drawing program.

Antibody characterization and specificity

The antibodies used and associated details are listed in the text and table 1 of Dell et al. (2016), apart from the orexin-A antibody. To reveal neurons that produce orexin as a neuropeptide/neurotransmitter, we used the AB3704 anti-Orexin-A rabbit polyclonal antibody from Merck-Millipore (AB3704, Merck-Millipore; RRID AB_91545) at a dilution of 1:3,000. The pattern of staining of orexinergic neurons in the hypothalamus found in the minke whale was similar to that seen in other mammals (Li and Kiruoac, 2008) and specifically the harbor porpoise and giraffe (e.g., Dell et al., 2012).

Stereological analysis

The numbers of cholinergic-immunopositive neurons (ChAT) in the LDT and PPT as well as the number of noradrenergic-immunopositive neurons (TH) in the LC and the number of orexinergic-immunopositive neurons (OxA) in the hypothalamus were determined with stereological techniques. An Olympus BX-60 light microscope equipped with a three axis motorized stage, video camera, and integrated Stereo-Investigator software (MicroBrightfield, Colchester, VT, v. 8.0) was used for the stereological counts. Independent pilot studies for LDT, PPT, LC, and hypothalamus were conducted on individual brain slices to optimize sampling parameters for cell counting (Table 1). Counting frames and grid sizes were optimized to achieve a mean coefficient of error of 10% or less (Gunderson and Jensen, 1987), while a guard zone of 5 μm was employed to avoid the introduction of errors due to sectioning artifacts (West et al., 1991). Section thickness was measured at every fifth sampling site and the number of immunopositive neurons were counted in accordance with the principles of the optical fractionator method (West et al., 1991). In PPT, hypothalamus, and LC a standardized stereological approach using simple random sampling was implemented with counting frames of 200 × 200 μm for PPT and hypothalamus and 150 × 150 μm for the LC. Corresponding grid sizes of 800 × 800 μm were used for PPT, LC, and the hypothalamus (Table 1). Due to the relatively small size of the LDT nucleus, we used a modified unbiased stereological approach by performing exhaustive total counts using a counting frame and grid size of 200 × 200 μm. The “optical fractionator” method was used to computationally determine the number of ChAT + neurons in the LDT and PPT as well as the number of TH + neurons in the LC and the OxA + neurons in the hypothalamus using the following formula:

$$N = Q/(SSF \times ASF \times TSF)$$

where N is the total estimated neuronal number, Q is the number of neurons counted, SSF is the section sampling fraction, ASF is the area subfraction (this was the ratio of the size of the counting frame to the size of the sampling grid), and TSF is the thickness subfraction (this was the ratio of the dissector height relative to cut section thickness) (Table 1). In order to determine TSF we used the average mounted section thickness calculated for each

individual, subtracted the total vertical guard zones (10 μm) to give dissector height, and used the ratio of dissector height to cut section thickness (50 μm) to provide TSF for each individual. The “nucleator probe” was used to estimate the mean volume and cross-sectional area of the immunopositive neurons and was used in conjunction with fractionator sampling (Gundersen, 1988).

RESULTS

The minke whale studied exhibited a range of nuclei involved in the regulation and initiation of the various phases of the sleep–wake cycle that were very similar to that observed in most mammals previously studied (Maseko et al., 2007; Dell et al., 2010, 2012, 2015b; Bhagwandin et al., 2013). This similarity extends to the locations of cell and terminal networks of the various GABAergic neurons examined (Bhagwandin et al., 2013; Dell et al., 2016).

Cholinergic nuclei of the basal forebrain and pons

The cholinergic nuclei of the basal forebrain and pons related to the regulation and initiation of the sleep–wake cycle identified in the minke whale include the diagonal band of Broca, islands of Calleja / olfactory tubercle, and nucleus basalis in the basal forebrain (Fig. 1A–D), and the pedunculopontine tegmental nucleus (PPT) and laterodorsal tegmental nucleus (LDT) in the pons (Fig. 2A–G). The diagonal band of Broca was located in the ventromedial aspect of the cerebrum and anterior to the hypothalamus (Fig. 1A,B). It contained a moderate density of bipolar neurons, which were regarded as oval or spherical in shape. The dendrites of these neurons were arranged in a dorsoventral orientation and it was noted that these neurons were rather small in comparison to the neurons identified in other basal forebrain nuclei. The islands of Calleja and olfactory tubercle were identified in the anterior floor of the cerebral hemisphere, ventral to the nucleus accumbens and the small anterior commissure, but anterior to the hypothalamus (Fig. 1A–C). While clearly distinct islands of Calleja were not present, local densities of cholinergic neurons, within a larger region of high-density cholinergic neurons, likely represent the islands of Calleja and the neurons of the olfactory tubercle, respectively. These neurons were mostly spherical in shape and multipolar in type, but oval-shaped bipolar neurons were also observed. These neurons exhibited a rough dorsolateral dendritic orientation. The nucleus basalis was found ventral to the internal capsulem but dorsal to the olfactory tubercle, in a position lateral to the hypothalamus (Fig. 1B–D). The nucleus basalis contained a moderate density of oval-shaped bipolar (small somal size) and multipolar (large somal size) cholinergic neurons, and all these cells had dendrites that were oriented in a lateroventral plane.

The PPT nucleus was located within the lateral and ventral pontine tegmentum, extending from the level of the oculomotor nucleus to the trigeminal motor nucleus (Fig. 2A–H). Throughout this region a moderate to high density of ChAT + neurons were observed, and stereological analysis revealed that there were ~260,922 cholinergic neurons forming the PPT. These irregularly shaped multipolar neurons, exhibiting no specific dendritic orientation (Fig. 4A), had a mean somal volume of 3,168.54 μm^3 (SD ± 2,029.82) and a mean surface area of 1,227.13 μm^2 (SD ± 843.37) (Table 2). The LDT nucleus was

identified in the lateroventral periaqueductal and periventricular gray matter (Fig. 2D–G). A low to moderate density of ovoid-shaped bipolar and multipolar neurons, with no specific somal orientation, was observed intermingling with the catecholaminergic neurons of the locus coeruleus (A6d). Stereological analysis revealed a neuronal population estimate of 13,320 neurons within the LDT, and these neurons had a mean somal volume of 3,011.55 μm^3 (SD ± 1,983.19) and a mean surface area of 1,229.83 μm^2 (SD ± 618.39) (Table 2), making them very similar in size to the cholinergic neurons of the PPT.

Putative catecholaminergic nuclei of the locus coeruleus complex

The locus coeruleus complex was readily subdivided into four distinct nuclei that included the subcoeruleus compact (A7sc) and diffuse (A7d) portions, the diffuse portion of the locus coeruleus (A6d), and the fifth arcuate nucleus (A5) (Fig. 2D–I). No distinct dorsal medial division of locus coeruleus (A4) could be identified in the minke whale, similar to the bottlenose dolphin (Manger et al., 2003), but different from the harbor porpoise where this nucleus was present (Dell et al., 2015b). The A7sc was located within the dorsal pontine tegmentum, immediately adjacent to the A6d nucleus in the ventrolateral periventricular gray matter. The A7sc contained a moderate to high density of tyrosine hydroxylase-immunopositive oval-shaped bipolar neurons that exhibited a medioventral dendritic orientation (Fig. 5A). The bipolar neurons forming the A7d were found throughout the lateral and ventral pontine tegmentum anterior to the trigeminal motor nucleus and extending around the superior cerebellar peduncle. Although the A7d is continuous with the A7sc, the density of A7d neurons decreased with distance from A7sc, making a moderate density of neurons throughout this nucleus. As mentioned, the A6d nucleus was found within the ventrolateral pontine periventricular gray matter (Fig. 2E–H), in a region where the cholinergic LDT neurons were also found. The A6d nucleus contained a moderate to high density of multipolar neurons that exhibited a dorsolateral dendritic orientation. A small number of tyrosine hydroxylase-immunopositive neurons found medial to the trigeminal sensory and motor nuclei (Fig. 2F–I) were assigned to the A5 nucleus. Stereological analysis revealed that the locus coeruleus complex as a whole contained ~203,686 neurons, with a mean somal volume of 1,957.65 μm^3 (SD ± 182.09) and an average surface area of 824.54 μm^2 (SD ± 309.73) (Table 2). These noradrenergic neurons were substantially smaller than the cholinergic neurons of the PPT and LDT that were found in a similar region of the brain.

Serotonergic nuclei of the dorsal raphe complex

The dorsal raphe complex was located mostly within the ventromedial portions of the periaqueductal gray matter, but neurons of certain divisions of this nucleus were found in the dorsal pontine tegmentum and dorsal periventricular gray matter (Fig. 2C–G). The dorsal raphe nuclear complex was comprised of six distinct divisions, the interfascicular (DRif), ventral (DRv), dorsal (DRd), lateral (DRl), peripheral (DRp), and caudal (DRc) divisions. The DRif nucleus was located between the two medial longitudinal fasciculi and contained a moderate to high density of oval bipolar neurons that had a dorsoventral dendritic orientation. The DRv nucleus was identified in the ventromedial region of the periaqueductal gray matter, immediately dorsal to the DRif. The DRv contained a low to moderate density of ovoid-shaped multipolar serotonergic neurons that exhibited no specific dendritic

orientation. The DRd was located dorsal to the DRv within the medial periaqueductal gray matter. The cell morphology and dendritic orientation of the DRd neurons resembled those seen in the DRv, but the DRd contained a higher density of serotonergic neurons. The DRl nucleus was found dorsolateral to both the DRd and DRv within the periaqueductal gray matter close to the ventrolateral edge of the cerebral aqueduct. The serotonergic neurons of the DRl were low in density, but were markedly larger than those of the DRd, DRv, and DRif, were multipolar, but exhibited no specific dendritic orientation. The DRp division of the dorsal raphe was located in the ventrolateral portion of the periaqueductal gray matter, anterior to the LDT and A6d, but several neurons of this nucleus were also observed in the dorsal tegmentum, anterior to the PPT and A7sc. A moderate to high density of ovoid-shaped multipolar neurons, all displaying no specific dendritic orientation, was observed within this nucleus. Interestingly, this division of the dorsal raphe complex appeared to have substantially more neurons than seen in other mammals, but was similar to this division in the harbor porpoise (Dell et al., 2015b). The DRc division was located within the most caudal region of the medial periaqueductal gray matter extending into the medial periventricular gray matter. This division appears to be a caudal extension of the DRl, where the neurons of the anterior bilateral DRl subdivisions merge. Within the DRc a low density of serotonergic multipolar neurons with a similar morphology to those seen in the DRl was observed.

Orexinergic nuclei of the hypothalamus

In cetartiodactyls, the orexinergic nuclei can be divided into parvocellular (one medial cluster) and magnocellular (main, zona incerta, and optic tract) clusters due to distinguishable size and topographical differences found within the hypothalamus (Dell et al., 2012). In this sense the minke whale exhibits the same parcellation of orexinergic neurons as observed in other cetaceans and artiodactyls (Fig. 1E–H). In the minke whale, the main cluster was located within the perifornical region and the lateral hypothalamus. The main cluster contained a high density of magnocellular orexin-A-immunopositive neurons that were either fusiform-shaped bipolar or triangular-shaped multipolar neurons, with similar somal sizes, and no specific dendritic orientation was noted (Fig. 7A). The optic tract nucleus was located in the lateral and ventral portions of the hypothalamus, in a location dorsal to the optic tract (Fig. 1D–G). It contained a low density of magnocellular orexinergic neurons that exhibited a similar morphology to those found in the main cluster, except that many of these neurons exhibited a horizontal dendritic orientation. The zona incerta cluster was identified within dorsolateral portions of the hypothalamus, with some neurons extending laterally beyond the borders of the hypothalamus to invade the region near the zona incerta (Fig. 1B–E). Although the zona incerta contained a low density of magnocellular orexinergic neurons, these neurons evinced a similar morphology to neurons found in both the main and optic tract clusters, but many neurons had a dendritic orientation that ran parallel to the ventral edge of the dorsal thalamus. Stereological analysis of the three magnocellular clusters revealed a mean population of 125,194 neurons that had a mean somal volume of 4,719.90 μm^3 (SD ± 1,456.15) and an average surface area of 2,083.42 μm^2 (SD ± 604.30) (Table 2).

The parvocellular orexinergic neurons formed a distinct cluster within the medial zone of the hypothalamus, between the small fornix and the lateral wall of the third ventricle (Fig. 1D–G). The parvocellular cluster contained a moderate to high density of fusiform-shaped bipolar neurons, and while some of these neurons exhibited a dorsoventral dendritic orientation, the majority exhibited no specific dendritic orientation. These parvocellular orexinergic neurons were visually smaller than the magnocellular neurons, and this qualitative assessment was confirmed by a stereological analysis that revealed that the mean neuron volume was 1,790.43 μm^3 (SD ± 612.22), and the mean surface area was 864.69 μm^2 (SD ± 318.71) (Table 2). Thus, the parvocellular orexinergic neurons are ~2.5 times smaller than the magnocellular orexinergic neurons. Interestingly, the stereological estimate of the population of parvocellular orexinergic neurons was 152,410 neurons, indicating that there are markedly more parvocellular orexinergic neurons in the minke whale than magnocellular orexinergic neurons.

Neurons and terminal networks containing calcium-binding proteins

Immunohistochemistry for the calcium-binding proteins calbindin (CB), calretinin (CR) and parvalbumin (PV) was performed to label subtypes of GABAergic neurons that are active during different sleep–wake states and during transitions between these states (Siegel, 2004; Jones, 2007; Bhagwandin et al., 2013). The results below, summarized in Table 3, detail the density of neurons and terminal networks immunopositive for CB, CR, and PV in relation to the sleep–wake related nuclei associated with the cholinergic, catecholaminergic, serotonergic, and orexinergic systems as well as the thalamic reticular nucleus.

Neurons and terminal networks containing calcium-binding proteins in the basal forebrain and pontine cholinergic system

A low density of CB-immunopositive neurons, coupled with a high density CB-immunopositive terminal network, was identified in the diagonal band of Broca. Both the nucleus basalis and the islands of Calleja / olfactory tubercle contained a high density of CB-immunopositive neurons and terminal network. A low density of CR-immunopositive neurons and a low density CR-immunopositive terminal network was observed in both the diagonal band of Broca and the islands of Calleja / olfactory tubercle. In contrast, the nucleus basalis contained a moderate density of CR-immunopositive neurons and a moderately dense CR-immunopositive terminal network. A low density of PV-immunopositive neurons was observed in the diagonal band of Broca and the islands of Calleja / olfactory tubercle, while the nucleus basalis exhibited a moderate density of PV-immunopositive neurons. All three basal forebrain cholinergic nuclei evinced a low density PV-immunopositive terminal network.

A moderate density of CB-immunopositive neurons, coupled with a high-density CB-immunopositive terminal network was observed in both the LDT and PPT (Fig. 4C). A high density of CR-immunopositive neurons associated with a high-density CR-immunopositive terminal network was observed in the PPT (Fig. 4D), while a moderate density of CR-immunopositive neurons and a moderately dense CR-immunopositive terminal network were observed in the LDT. A low density of PV-immunopositive neurons was found in both the LDT and PPT, while a moderately dense PV-immunopositive terminal network

density was observed in the LDT, while the PPT exhibited a low-density PV-immunopositive terminal network (Fig. 4B).

Neurons and terminal networks containing calcium-binding proteins in the locus coeruleus complex

A low density of CB-immunopositive neurons were identified in both the A7sc (Fig. 5C) and A7d, while the A6d had a moderate density of CB-immunopositive neurons. The densities of the CB-immunopositive terminal networks were different between these three nuclei, with the A7sc having a moderately dense CB-immunopositive terminal network (Fig. 5C), the A7d having a low density, and the A6d having a high-density CB-immunopositive terminal network. A low density of CR-immunopositive neurons were identified in the A7sc (Fig. 5D), while both the A7d and A6d exhibited a moderate density of CR-immunopositive neurons. Again, the density of the CR-immunopositive network differed between the three nuclei, with the A7sc having a low density (Fig. 5D), the A7d a moderate density, and the A6d having a high-density terminal network. No PV-immunopositive neurons were observed throughout the A7d, while in both the A7sc (Fig. 5B) and the A6d only occasional PV-immunopositive neurons were observed. In the A7sc (Fig. 5B) and the A6d a moderately dense PV-immunopositive terminal network was observed, while in the A7d a low density PV-immunopositive terminal network was observed.

Neurons and terminal networks containing calcium-binding proteins in the dorsal raphe complex

The majority of the subdivisions of the dorsal raphe complex exhibited a moderate density of CB-immunopositive neurons, while the DRif had a low density and the DRp had a high density of CB-immunopositive neurons. The majority of divisions exhibited a high-density CB-immunopositive terminal network, but DRif had a moderate density and the DRv a low-density CB-immunopositive terminal network. The DRp was the only subdivision that contained both a high density of CB-immunopositive neurons and a high-density CB-immunopositive terminal network. A moderate density of CR-immunopositive neurons was observed throughout most of the subdivisions, but the DRl had a high density of CR-immunopositive neurons. Three subdivisions, the DRif, DRd, and DRd, all exhibited a moderately dense CR-immunopositive terminal network, while the DRl, DRp, and DRc exhibited a high-density CR-immunopositive terminal network. No parvalbumin-immunopositive neurons were observed in the DRif or the DRc, while the remaining subdivisions exhibited a low density of PV-immunopositive neurons. The DRif lacked a PV-immunopositive terminal network, while the remaining subdivisions all exhibited a low density PV-immunopositive terminal network.

Neurons and terminal networks containing calcium-binding proteins in the hypothalamic orexinergic clusters

A high density of CB-immunopositive neurons was observed in both the main (Fig. 7C) and zona incerta magnocellular orexinergic clusters, while a moderate density of CB-immunopositive neurons were observed in the optic tract cluster and the medially located parvocellular orexinergic cluster. In all three magnocellular clusters, a moderately dense CB-immunopositive terminal network was observed (Fig. 7C), while the medially located

parvocellular cluster evinced a high density CB-immunopositive terminal network. The main cluster exhibited a low density of CR-immunopositive neurons (Fig. 7D), while the remaining clusters all had a high density of CR-immunopositive neurons. Both the main cluster (Fig. 7D) and the zona incerta cluster had a moderately dense CR-immunopositive terminal network, while the optic tract and parvocellular clusters had high-density CR-immunopositive terminal networks. A low density of PV-immunopositive neurons was observed in the main (Fig. 7B) and optic tract clusters, while no PV-immunopositive neurons were observed in the regions where the zona incerta and parvocellular orexinergic clusters were located. The optic tract cluster evinced a moderately dense PV-immunopositive terminal network, the main (Fig. 7B) and parvocellular clusters housed low-density PV-immunopositive terminal networks, while no PV-immunopositive terminal network was found in the zona incerta cluster.

Neurons and terminal networks containing calcium-binding proteins in thalamic reticular nucleus

The thalamic reticular nucleus of the minke whale occupied a position typical of mammals (Fig. 8). Within this nucleus occasional CB-immunopositive neurons (Fig. 8C), a low density of CR-immunopositive neurons (Fig. 8D), and a moderate density of PV-immunopositive neurons (Fig. 8B) were observed. A low-density CB-immunopositive terminal network (Fig. 8C), a moderately dense CR-immunopositive terminal network (Fig. 8D), and a high-density PV-immunopositive terminal network (Fig. 8B) were observed within the thalamic reticular nucleus of the minke whale.

DISCUSSION

The current study examined the neural systems related to the control and regulation of sleep and wake in the minke whale and compares these to published findings in odontocete cetaceans and other mammals to provide a more holistic understanding of cetacean sleep phenomenology. The nuclear organization of the cholinergic, catecholaminergic, serotonergic, and orexinergic systems in the minke whale were similar to earlier findings in the harbor porpoise (Dell et al., 2012, 2016) as well as previous terrestrial mammals studied (Maseko et al., 2007; Dell et al., 2010, 2013; Krüger et al., 2010a,b; Calvey et al., 2013). Additionally, the putative GABAergic system, identified with immunohistochemistry to the calcium-binding proteins parvalbumin, calbindin, and calretinin, in the minke whale displayed a similar morphology and organization to that seen in the harbor porpoise (Dell et al., 2016) and to terrestrial mammals previously studied (Bhagwandin et al., 2013). Minor differences in the appearance of the GABAergic systems between the minke whale and harbor porpoise can be explained as a result of brain size differences between these species. As limited studies of sleep are available for the mysticetes, it is assumed that these marine mammals also undergo USWS like their odontocete counterparts (Lyamin et al., 2008), and the findings of the current study support this supposition.

Similarities in the nuclear organization of the sleep-related neural systems across mammals

In the current study the neural sleep systems of the cholinergic basal forebrain and pons, the noradrenergic nuclei of the pons, the serotonergic dorsal raphe, and the hypothalamic orexinergic system in the minke whale were found to be very similar to those studied in the harbor porpoise (Dell et al., 2012, 2016) and the locus coeruleus of the bottlenose dolphin (Manger et al., 2003). Thus, these neural systems involved in the control and regulation of sleep and wake displayed similar locations, nuclear parcellation, and neuronal morphology in the minke whale, harbor porpoise, and bottlenose dolphin. Furthermore, these systems in the minke whale had a similar nuclear organization to that seen in terrestrial mammals previously studied (Maseko et al., 2007; Dell et al., 2010; Calvey et al., 2013), the only exception being the additional orexinergic parvocellular neural cluster in the minke whale, which is found in Cetartiodactyls and the African elephant (Dell et al., 2012; Maseko et al., 2013). As the aquatic cetaceans and terrestrial mammals exhibit quite different sleep physiology, the fact that the nuclei involved in the control and regulation of sleep are so similar, without the addition of novel nuclei, or the deletion of specific nuclei, we can infer that the neural control of the sleep–wake cycle across mammals is a strongly conserved evolutionary trait (Tobler, 1995; Rattenborg et al., 2000; Lyamin et al., 2008). Similar to our earlier study on the harbor porpoise (Dell et al., 2016), there are no qualitative changes in the sleep-associated neural systems in the minke whale that indicates potential differences in their sleep physiology to either other cetaceans, or indeed other mammals.

Similarities of the GABAergic systems in sleep-associated nuclei across mammals

GABAergic neurons associated with the sleep-related nuclei are considered to function as promoters of sleep (Siegel, 2004; Datta and MacLean, 2007). In this study the GABAergic neurons and terminal networks were studied by examining the localization of the calcium-binding proteins (parvalbumin, calbindin, and calretinin) (Bhagwandin et al., 2013) and provided the first report of the organization of the putative GABAergic system in a mysticete whale. It was noted that the location of putative GABAergic neurons and terminal networks in the sleep–wake-associated nuclei was similar to that seen in the harbor porpoise (Dell et al., 2016) and terrestrial mammals previously studied (Bhagwandin et al., 2013). Despite this overall similarity, some differences in neuronal and terminal network densities were noted when comparing the minke whale with the harbor porpoise. The minke whale exhibited a higher calbindin terminal network density in the cholinergic nuclei of the basal forebrain and pons, as well as a higher calretinin neuronal and terminal network density in the cholinergic nuclei of the pons. The cholinergic pontine nuclei serve as a relay control for the regulation of cortical activation and arousal (Sarter and Bruno, 2000; Dringenberg and Olmstead, 2003), and in a volumetrically large brain, such as that of the minke whale, higher densities of calbindin and calretinin neurons and terminal networks may be required to provide appropriate inhibition in the control of cortical arousal. There were marked increases in the density of calbindin and calretinin neurons and terminal networks within the hypothalamic orexinergic system of the minke whale when compared to the harbor porpoise (Dell et al., 2016). One could speculate that as the minke whale is an opportunistic feeder (Horwood, 1990), it would have a greater appetitive drive, and thus would require more

stringent control of the orexinergic system, particularly the parvocellular cluster (Dell et al., 2012).

The minke whale exhibited lower densities of calbindin neurons and terminal networks within the locus coeruleus complex when compared to the harbor porpoise. This difference, however, appears to be related to the larger size of this region of the brain in the minke whale compared to the harbor porpoise. There was a reduced number of calretinin neurons in the thalamic reticular nucleus of the minke whale when compared to the harbor porpoise (Dell et al., 2016), but again, this qualitative difference in cell density may be related to the larger size of this structure in the minke whale. The location and density of parvalbumin-immunopositive neurons and terminal networks was similar in the harbor porpoise and terrestrial mammals (Dell et al., 2016), but the minke whale exhibited slight increases in the densities of the parvalbumin terminal networks in the locus coeruleus complex and the hypothalamic orexinergic system, as well as a slight increase in parvalbumin neuronal density in the pontine cholinergic nuclei. These features may, speculatively, indicate more stringent neuronal control of the activity of these cholinergic, noradrenergic, and orexinergic neurons in the minke whale compared to other mammals.

Orexinergic system in the minke whale

The parcellation of clusters of orexinergic neurons in the hypothalamus, and their general arrangement, is very similar to that seen in the harbor porpoise, giraffe (Dell et al., 2012), and African elephant (Maseko et al., 2013). Additionally, the morphology and density of the orexinergic terminal networks in the anterior cingulate and occipital cerebral cortex of the minke whale is identical to that seen in the harbor porpoise, but lower in density than that seen in artiodactyls (Dell et al., 2015). In these senses, the orexinergic system of the minke whale is very similar to that of the harbor porpoise, and distinguishes the cetaceans from the artiodactyls and other mammals. In the current study we estimated that the minke whale has ~277,604 orexinergic neurons (those immunopositive to the orexin-A antibody) in the hypothalamus, 125,194 of which were magnocellular and 152,410 of which were parvocellular. This number of orexinergic neurons is far higher than seen in the harbor porpoise, which had 21,254 orexinergic neurons in total, 10,419 of which were magnocellular and 10,834 being parvocellular (Dell et al., 2012). In the minke whale, for every magnocellular orexinergic neuron there are 1.22 parvocellular neurons, and in the harbor porpoise there are 1.04 parvocellular neurons for each magnocellular neuron. In the giraffe brain there are 15,003 orexinergic neurons (7,327 magnocellular and 7,676 parvocellular, a ratio of 1.05) (Dell et al., 2012), while in the human brain there are varying counts of orexinergic neurons, ranging from around 15,000–20,000 (Kilduff and Peyron, 2000) up to around 70,000 (Thannickal et al., 2000; Henny and Jones, 2006). Thus, the harbor porpoise and giraffe have fewer orexinergic neurons than humans, but the minke whale has significantly more. Even if we only look at the magnocellular orexinergic neurons, which are likely to be the homologous neurons to those found in humans, the minke whale still has around 55,000 more orexinergic neurons than humans. Despite this large number of orexinergic neurons, the orexinergic bouton terminal network density in the minke whale is no different from that seen in the harbor porpoise, and less dense than the giraffe and other artiodactyls (Dell et al., 2015). Given this, it is difficult to speculate

why the minke whale has such an inflated number of orexinergic neurons compared to other large-brained species. Part of the difference may be accounted for by allometric scaling, where larger brains generally have more neurons than smaller brains (Herculano-Houzel et al., 2014), but this would not account for the radical difference seen in the minke whale compared to other species. A full allometric study of quantified orexinergic neuronal numbers across a range of species, especially artiodactyls and other cetaceans, is required to provide the proper context in which to interpret the results of the orexinergic system in the minke whale. Until this is achieved, discussing the function of this seemingly supernumerary system in the minke whale will only be speculative, although it would seem that this may relate to the dietary requirements and appetitive drive needed to sustain such a large body mass (Dell et al., 2012).

Does the minke whale sleep like an odontocete cetacean?

Studies of sleep in mysticete whales are limited to behavioral observations made on a gray whale calf (Lyamin et al., 2000, 2001). While this study is suggestive of the mysticete whales showing the same sleep phenomenology as the well-studied odontocete cetaceans (Lyamin et al., 2008), the results are not particularly clear. Undertaking electrophysiological studies of sleep in the large baleen whales, while technically possible, is practically unfeasible at the present time; however, as undertaken in this study, we can examine the structure of the brain to search for clues relating to how sleep might occur in the mysticete whales. In a previous study on the brain of the harbor porpoise, we proposed that a suite of quantitative changes in certain regions of the odontocete brain associated with the regulation and control of sleep and wake, rather than changes in qualitative features, are likely to account for the production of USWS and suppressed REM sleep, the sleep typically observed in odontocete cetaceans (Dell et al., 2016). These features included small telencephalic commissures, a large posterior commissure, supernumerary cholinergic and noradrenergic neurons in the pons, as well as an expanded peripheral division of the dorsal raphe nuclei.

In this sense we can examine the findings on the minke whale brain to determine if these features, which appear to be different to bihemispheric sleeping mammals, are present. The three main telencephalic commissures, the anterior commissure, corpus callosum, and hippocampal commissure are all small in the minke whale, like that observed in the harbor porpoise and other odontocete cetaceans (Wilson, 1933; Lyamin et al., 2008; Manger et al., 2010; Ratner et al., 2011; Patzke et al., 2015), while quantification of axonal numbers in the corpus callosum have shown that they are low in the minke whale (Ratner et al., 2011). As observed in other mysticete whales (Lyamin et al., 2008), we noted in the present study a large posterior commissure in the minke whale. Within the pontine region, the minke whale, with its ~3 kg brain, had 274,242 cholinergic neurons in the LDT+PPT, and 203,686 noradrenergic neurons in the locus coeruleus complex. In comparison, the harbor porpoise with a 500 g brain had 126,776 cholinergic neurons in the LDT+PPT and 122,878 locus coeruleus neurons (Dell et al., 2016), while the human brain, at around 1.4 kg, has ~20,000 pontine cholinergic neurons (Manaye et al., 1999) and 22,000 noradrenergic neurons (Mouton et al., 1994). Lastly, the peripheral division of the dorsal raphe nuclear

complex in the minke whale shows a similar morphology and neuronal density as seen in the harbor porpoise (Dell et al., 2016).

Thus, in the minke whale a similar suite of features related to the proposed control and regulation of sleep as seen in the harbor porpoise can be identified. As with the harbor porpoise, the expanded peripheral division of the dorsal raphe nuclear complex may act to suppress REM sleep in the minke whale. The small size, and limited numbers of axons, of the telencephalic hemispheres will contribute to the functional independence of the cerebral hemispheres. Lastly, the large posterior commissure and the supernumerary cholinergic and noradrenergic neurons in the pons will potentially, under input related to the drive for sleep derived in the cerebral hemispheres, determine when and which cerebral hemisphere enters slow wave sleep. This range of quantitative similarities between harbor porpoises and minke whales, which distinguish them from bihemispheric sleeping mammals, along with the behavioral observations of sleep the gray whale, all point to the likelihood of minke whales and other mysticete whales possessing the same sleep phenomenology studied in detail in odontocete cetaceans (Lyamin et al., 2008).

Further studies of the brains of other species of cetaceans and a range of artiodactyls are required to fully determine whether the suite of characters identified in the minke whale and harbor porpoise, proposed to be related to the production and control of USWS and the suppression of REM sleep, are truly characteristic of this group. For example, studies of the brain of the hippopotami, being the closest terrestrial relative of the cetaceans, would be of importance. In addition, a broader range of quantitative studies of the cholinergic, noradrenergic, serotonergic, and orexinergic systems are also needed, to properly determine the degree to which the numbers of neurons in cetaceans differ from the other artiodactyls. Lastly, a series of similar studies on other mammals that show the capacity for USWS, such as otariid seals, walruses, and the sirenians (Lyamin et al., 2008) in comparison to their close bihemispheric sleeping relatives in the carnivores and Afrotheria, may refine and help to understand the specific characters of the brain required to produce the unusual sleep phenomenology evidenced in odontocete cetaceans.

ACKNOWLEDGMENTS

We thank the Iceland Ministry of Fisheries and Agriculture for allowing us to obtain the specimens of minke whale brains.

Grant sponsor: South African National Research Foundation (Innovation scholarship to L.D.); Grant sponsor: Society, Ecosystems and Change; Grant number: SeaChange Grant KFD2008051700002 (to P.R.M.); Grant sponsor: ISN-CAEN travel grant (to L.D.); Grant sponsor: fellowship with the Postdoc-Programme of the German Academic Exchange Service, DAAD (to N.P.); Grant sponsor: Reykjavik University 2010 Development Fund (to K.Æ.K.); Grant sponsor: IOER R&G Grant from Des Moines University; Grant number: 12-13-03 (to M.A.S.); Grant sponsor: National Institutes of Health (NIH); Grant number: DA 2R01MH064109; Grant sponsor: Department of Veterans Affairs (to J.M.S.).

Abbreviations

III	oculomotor nucleus
IV	trochlear nucleus

3V	third ventricle
4V	fourth ventricle
3n	oculomotor nerve
5n	trigeminal nerve
A5	fifth arcuate nucleus
A6d	diffuse portion of locus coeruleus
A7d	nucleus subcoeruleus, diffuse portion
A7sc	nucleus subcoeruleus, compact portion
A8	retrorubral nucleus
A9pc	substantia nigra, pars compacta
A9l	substantia nigra, lateral
A9m	substantia nigra, medial
A9v	substantia nigra, ventral
A10	ventral tegmental area
A10c	ventral tegmental area, central
A10d	ventral tegmental area, dorsal
A10dc	ventral tegmental area, dorsal caudal
A11	caudal diencephalic group
A12	tuberal cell group
A13	zona incerta catecholaminergic nucleus
A14	rostral periventricular nucleus
A15d	anterior hypothalamic group, dorsal division
A15v	anterior hypothalamic group, ventral division
ac	anterior commissure
Arc	hypothalamic arcuate nucleus
B9	supralemniscal serotonergic nucleus
ca	cerebral aqueduct
cic	commissure of the inferior colliculus
CLi	caudal linear nucleus

Diag.B	diagonal band of Broca
DRc	dorsal raphe nucleus, caudal division
DRd	dorsal raphe nucleus, dorsal division
DRif	dorsal raphe nucleus, interfascicular division
DRl	dorsal raphe nucleus, lateral division
DRp	dorsal raphe nucleus, peripheral division
DRv	dorsal raphe nucleus, ventral division
DT	dorsal thalamus
EW	Edinger-Westphal nucleus
f	fornix
GC	central gray matter
Hyp	hypothalamus
Hyp.d	dorsal hypothalamic cholinergic nucleus
Hyp.l	lateral hypothalamic cholinergic nucleus
Hyp.v	ventral hypothalamic cholinergic nucleus
IC	inferior colliculus
ic	internal capsule
IP	interpeduncular nucleus
IS.CALL/TOL	islands of Calleja and olfactory tubercle
LDT	laterodorsal tegmental nucleus
lfp	longitudinal fasciculus of the pons
Mc	main cluster of orexinergic neurons
mcp	middle cerebellar peduncle
mlf	medial longitudinal fasciculus
MnR	median raphe nucleus
N.Acc	nucleus accumbens
N.Bas	nucleus basalis
N.Ell	nucleus ellipticus
NSp	nigrostriatal pathway

OC	optic chiasm
OT	optic tract
Otc	optic tract cluster of orexinergic neurons
P	putamen nucleus
PBg	parabigeminal nucleus
PC	cerebral peduncle
Pc	parvocellular cluster of orexinergic neurons
PPT	pedunculopontine tegmental nucleus
Rmc	red nucleus, magnocellular division
RMR	rostral mesencephalic raphe cluster
RtTg	reticulotegmental nucleus
SC	superior colliculus
scp	superior cerebellar peduncle
SON	supraoptic nucleus
Stn	subthalamic nucleus
Vmot	trigeminal motor nucleus
TOL	olfactory tubercle
VPO	ventral pontine nucleus
Vs	trigeminal sensory nucleus
xscp	decussation of the superior cerebral peduncle
Zic	zona incerta cluster of orexinergic neurons

LITERATURE CITED

Bhagwandin A, Gravett N, Bennett NC, Manger PR. 2013. Distribution of parvalbumin, calbindin and calretinin containing neurons and terminal networks in relation to sleep associated nuclei in the brain of the giant Zambian molerat (*Fukomys mechowii*). J Chem Neuroanat 52:69–79. [PubMed: 23796985]

Calvey T, Patzke N, Kaswera C, Gilissen E, Bennett NC, Manger PR. 2013. Nuclear organization of some immunohistochemically identifiable neural systems in three Afrotherian species–*Potomogale velox, Amblysomus hottentotus* and *Petrodromus tetradactylus*. J Chem Neuroanat 50-51:48–65. [PubMed: 23517750]

Datta S, MacLean RR. 2007. Neurobiological mechanisms for the regulation of mammalian sleep-wake behavior: reinterpretation of historical evidence and inclusion of contemporary cellular and molecular evidence. Neurosci Biobehav Rev 31:775–824. [PubMed: 17445891]

Dell LA, Kruger JL, Bhagwandin A, Jillani NE, Pettigrew JD, Manger PR. 2010. Nuclear organization of cholinergic, putative catecholaminergic and serotonergic systems in the brains of two megachiropteran species. J Chem Neuroanat 40:177–195. [PubMed: 20566331]

Dell LA, Patzke N, Bhagwandin A, Bux F, Fuxe K, Barber G, Siegel JM, Manger PR. 2012. Organization and number of orexinergic neurons in the hypothalamus of two species of Cetartiodactyla: A comparison of giraffe (*Giraffa camelopardalis*) and harbour porpoise (*Phocoena phocoena*). J Chem Neuroanat 44:98–109. [PubMed: 22683547]

Dell LA, Kruger JL, Pettigrew JD, Manger PR. 2013. Cellular location and major terminal networks of the orexinergic system in the brain of two megachiropterans. J Chem Neuroanat 53:64–71. [PubMed: 24041616]

Dell LA, Spocter MA, Patzke N, Karlson KÆ, Alagaili AN, Bennett NC, Muhammed OB, Bertelsen MF, Siegel JM, Manger PR. 2015. Orexinergic bouton density is lower in the cerebral cortex of cetaceans compared to artiodactyls. J Chem Neuroanat 68:61–76. [PubMed: 26232521]

Dell LA, Patzke N, Spocter MA, Siegel JM, Manger PR. 2016. Organization of the sleep-related neural systems in the brain of the harbor porpoise (*Phocoena phocoena*). J Comp Neurol [Epub ahead of print].

Dringenberg HC, Olmstead MC. 2003. Integrated contributions of the basal forebrain and thalamus to neocortical activation elicited by pedunculopontine tegmental stimulation in urethane-anesthetized rats. Neuroscience 119:839–853. [PubMed: 12809705]

Eriksen N, Pakkenberg B. 2007. Total neocortical cell number in the mysticete brain. Anat Rec 290:83–95.

Gundersen HJ. 1988. The nucleator. J Microsc 151:3–21. [PubMed: 3193456]

Gundersen HJ, Jensen EB. 1987. The efficiency of systematic sampling in stereology and its prediction. J Microsc 147:229–263. [PubMed: 3430576]

Henny P, Jones BE. 2006. Innervation of orexin/hypocretin neurons by GABAergic, glutamatergic or cholinergic basal forebrain terminals evidenced by immunostaining for presynaptic vesicular transporter and postsynaptic scaffolding proteins. J Comp Neurol 499:645–661. [PubMed: 17029265]

Herculano-Houzel S, Manger PR, Kaas JH. 2014. Brain scaling in mammalian evolution as a consequence of concerted and mosaic changes in numbers of neurons and average neuronal cell size. Front Neuroanat 8:77. [PubMed: 25157220]

Horwood J. 1990. Biology and exploitation of the minke whale. Boca Raton, FL: CRC Press.

Jones EG. 2007. The thalamus. Cambridge, UK: Cambridge University Press.

Kilduff TS, Peyron C. 2000. The hypocretin/orexin ligand-receptor system: implications for sleep and sleep disorders. Trends Neurosci 23:359–365. [PubMed: 10906799]

Kot BW, Sears R, Anis A, Nowacek DP, Gedamke J, Marshall CD. 2012. Behavioral responses of minke whales (*Balaenoptera acutorostrata*) to experimental fishing gear in a coastal environment. J Exp Marine Biol Ecol 413:13–20.

Krüger JL, Dell LA, Bhagwandin A, Jillani NE, Pettigrew JD, Manger PR. 2010a. Nuclear organization of cholinergic, putative catecholaminergic and serotonergic systems in the brains of five microchiropteran species. J Chem Neuroanat 40:210–222. [PubMed: 20566329]

Krüger JL, Dell LA, Pettigrew JD, Manger PR. 2010b. Cellular location and major terminal networks of the orexinergic system in the brains of five microchiropteran species. J Chem Neuroanat 40:256–262. [PubMed: 20654711]

Li S, Kiruoac J. 2008. Projections from the paraventricular nucleus of the thalamus to the forebrain, with special emphasis on the extended amygdala. J Comp Neurol 506:263–287. [PubMed: 18022956]

Lyamin OI, Manger PR, Mukhametov LM, Siegel JM, Shpak OV. 2000. Rest and activity states in a grey whale. J Sleep Res 9:261–267. [PubMed: 11012865]

Lyamin OI, Mukhametov LM, Siegel JM, Manger PR, Shpak OV. 2001. Resting behavior in a rehabilitating gray whale calf. Aquat Mamm 27:256–266.

Lyamin OI, Mukhametov LM, Siegel JM, Nazarenko EA, Polyakova IG, Shpak OV. 2002. Unihemispheric slow wave sleep and the state of the eyes in a white whale. Behav Brain Res 129:125–129. [PubMed: 11809503]

Lyamin OI, Manger PR, Ridgway SH, Mukhametov LM, Siegel JM. 2008. Cetacean sleep: An unusual form of mammalian sleep. Neurosci Biobehav Rev 32:1451–1484. [PubMed: 18602158]

Manaye KF, Zweig R, Wu D, Hersh LB, De Lacalle S, Saper CB, German DC. 1999. Quantification of cholinergic and select non-cholinergic mesopontine neuronal populations in the human brain. Neuroscience 89:759–770. [PubMed: 10199611]

Manger PR, Ridgway SH, Siegel JM. 2003. The locus coeruleus complex of the bottlenose dolphin (*Tursiops truncatus*) as revealed by tyrosine hydroxylase immunohistochemistry. J Sleep Res 12:149–155. [PubMed: 12753352]

Manger PR, Hemingway J, Haagensen M, Gilissen E. 2010. Cross-sectional area of the elephant corpus callosum: comparison to other Eutherian mammals. Neuroscience 167:815–824. [PubMed: 20206234]

Manger PR, Prowse M, Haagensen M, Hemingway J. 2012. Quantitative analysis of neocortical gyrencephaly in African elephants (*Loxodonta africana*) and six species of cetaceans: comparison with other mammals. J Comp Neurol 520:2430–2439. [PubMed: 22237903]

Maseko BC, Bourne JA, Manger PR. 2007. Distribution and morphology of cholinergic, putative catecholaminergic and serotonergic neurons in the brain of the Egyptian Rousette flying fox, *Rousettus aegyptiacus*. J Chem Neuroanat 34:108–127. [PubMed: 17624722]

Maseko BC, Spocter MA, Haagensen M, Manger PR. 2011. Volumetric analysis of the African elephant ventricular system. Anat Rec 294:1412–1417.

Maseko BC, Spocter MA, Haagensen M, Manger PR. 2012. Elephants have relatively the largest cerebellum size of mammals. Anat Rec 295:661–672.

Maseko BC, Patzke N, Fuxe K, Manger PR. 2013. Architectural organization of the African elephant diencephalon and brainstem. Brain Behav Evol 82:83–128. [PubMed: 24021932]

Mouton PR, Pakkenberg B, Gundersen HJG, Price DL. 1994. Absolute number and size of pigmented locus coeruleus neurons in young and aged individuals. J Chem Neuroanat 7:185–190. [PubMed: 7848573]

Mukhametov LM, Supin AYa, Strokova IG. 1976. Interhemispheric asymmetry of cerebral functional states during sleep in dolphins. Dokl Akad Nauk SSSR 229:767–770. [PubMed: 976042]

Mukhametov LM, Supin AYa, Polyakova IG. 1977. Interhemispheric asymmetry of the electroencephalographic sleep pattern in dolphins. Brain Res 134:581–584. [PubMed: 902119]

Patzke N, Spocter MA, Karlsson KÆ, Bertelsen MF, Haagensen M, Chawana R, Streicher S, Kaswera C, Gilissen E, Alagaili AN, Mohammed OB, Reep RL, Bennett NC, Siegel JM, Ihunwo AO, Manger PR. 2015. In contrast to many other mammals, cetaceans have relatively small hippocampi that appear to lack adult neurogenesis. Brain Struct Funct 220:361–383. [PubMed: 24178679]

Ratner C, Riise J, Eriksen N, Pakkenberg B. 2011. A postmortem study of the corpus callosum in the common minke whale (*Balaenoptera acutorostrata*). Marine Mamm Sci 27:688–700.

Rattenborg NC, Amlaner CJ, Lima SL. 2000. Behavioral, neurophysiological and evolutionary perspectives on unihemispheric sleep. Neurosci Biobehav Rev 24:817–842. [PubMed: 11118608]

Sarter M, Bruno JP. 2000. Cortical cholinergic inputs mediating arousal, attentional processing, and dreaming: differential afferent regulation of the basal forebrain by telencephalic and brainstem afferents. Neuroscience 95:933–952. [PubMed: 10682701]

Siegel JM. 2004. The neurotransmitters of sleep. J Clin Psychiatry 65:4–7.

Thannickal TC, Moore RY, Nienhuis R, Ramanathan L, Gulyani S, Aldrich M, Cornford M, Siegel JM. 2000. Reduced number of hypocretin neurons in human narcolepsy. Neuron 27:469–474. [PubMed: 11055430]

Tobler I. 1995. Is sleep fundamentally different between mammalian species? Behav Brain Res 69:35–41. [PubMed: 7546316]

West MJ, Slomianka L, Gundersen HJ. 1991. Unbiased stereological estimation of the total number of neurons in the subdivisions of the rat hippocampus using the optical fractionator. Anat Rec 231:482–497. [PubMed: 1793176]

Wilson RB. 1933. The anatomy of the brain of the whale (*Balaenoptera sulfurea*). J Comp Neurol 58:419–480.

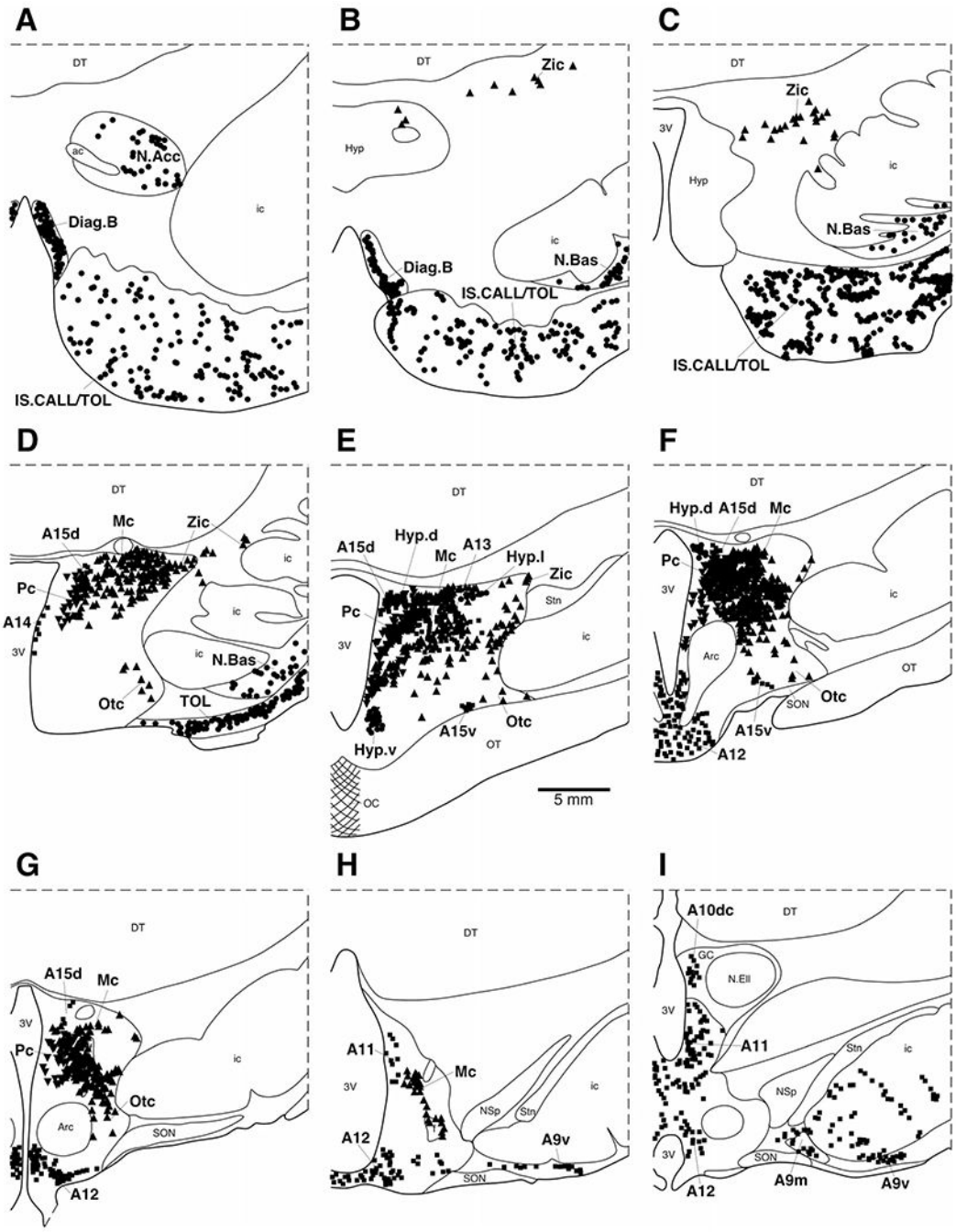

Figure 1.

Diagrammatic reconstruction of a series of coronal sections through the basal forebrain and diencephalon of the minke whale brain illustrating the location of choline acetyltransferase (ChAT, circles), tyrosine hydroxylase (TH, squares) magnocellular orexinergic (OxA, triangles), and parvocellular orexinergic (OxA, inverted triangles) immunoreactive neurons. Each symbol represents a single neuron. The outlines of the architectonic regions were drawn using Nissl and myelin stain and immunoreactive neurons marked on the drawings

from one animal. Figure **A** represents the most rostral section, **I** the most caudal. Each figure is ~2 mm apart. See list for abbreviations.

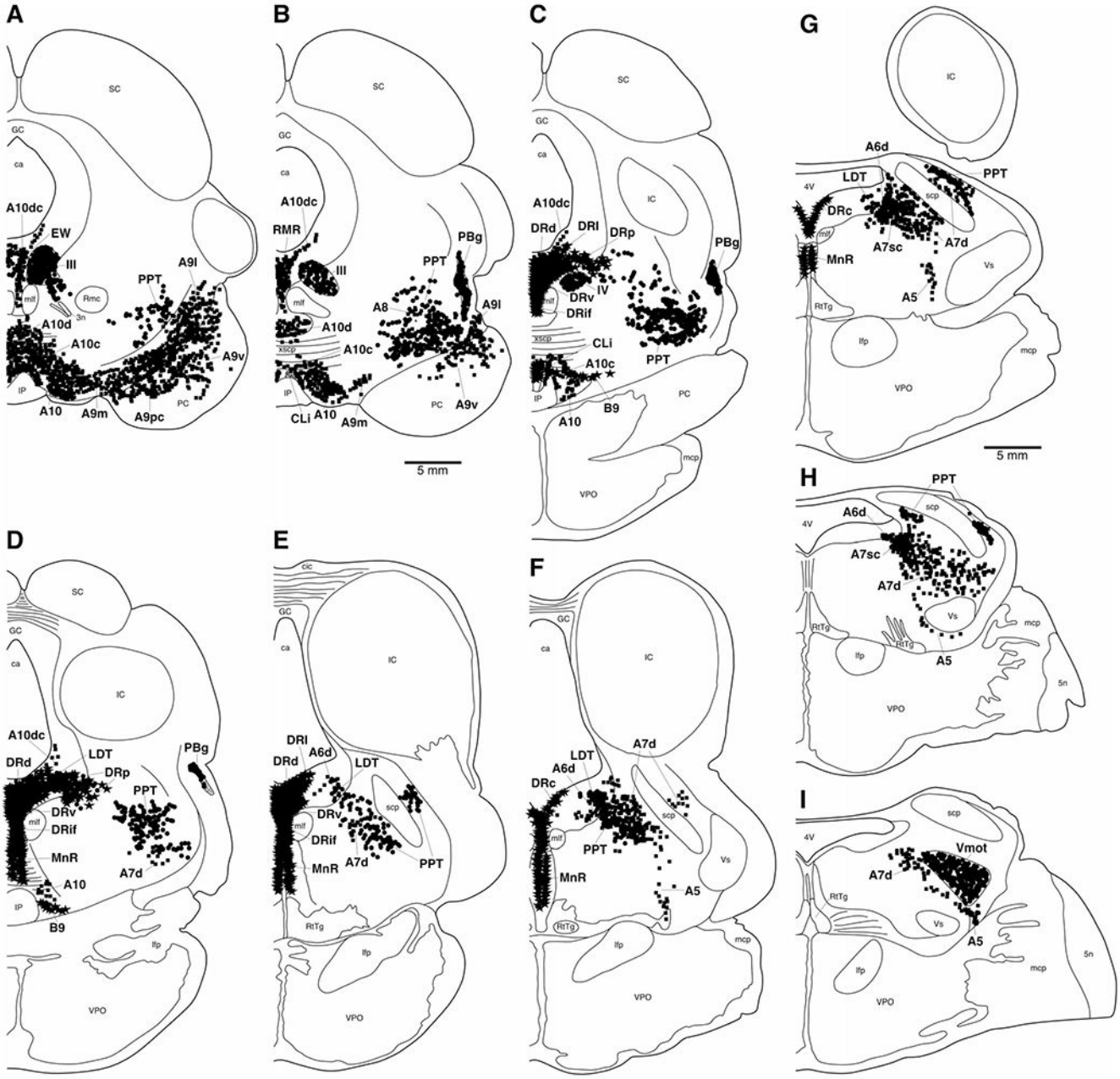

Figure 2.

Diagrammatic reconstruction of a series of coronal sections through the midbrain and pons of the minke whale brain illustrating the location of choline acetyltransferase (ChAT, circles), tyrosine hydroxylase (TH, squares), and serotonergic (stars) immunoreactive neurons. Each symbol represents a single neuron. The outlines of the architectonic regions were drawn using Nissl and myelin stain and immunoreactive neurons marked on the drawings from one animal. Figure **A** represents the most rostral section, **I** the most caudal. Each figure is ~2 mm apart. See list for abbreviations.

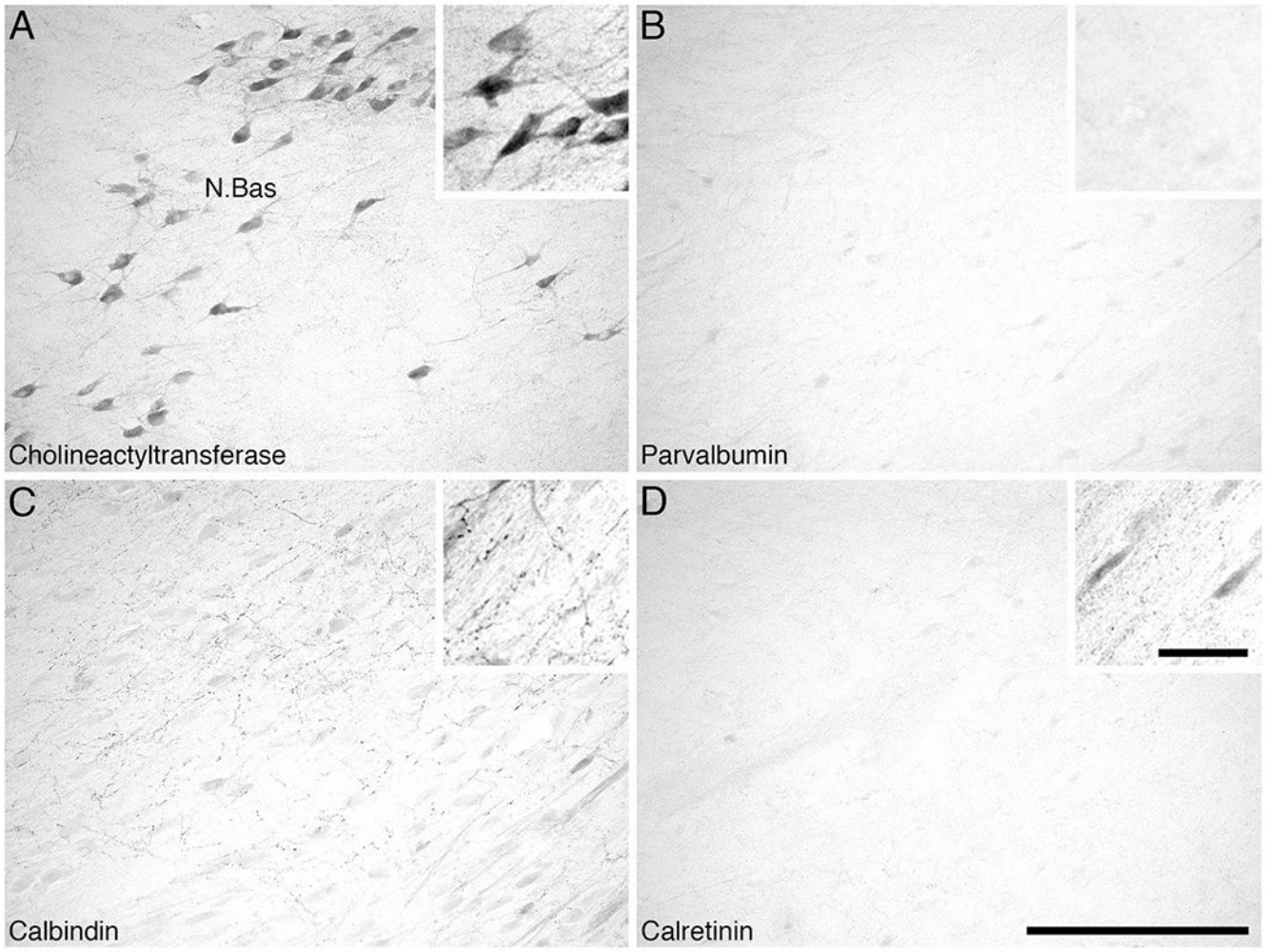

Figure 3.

Low (main image) and high (inset) magnification photomicrographs of the nucleus basalis (N.Bas) in the basal forebrain of the minke whale. **A:** Neurons immunoreactive for choline acetyltransferase showing part of the nucleus basalis (N.Bas). **B:** Parvalbumin immunoreactivity, note the absence of parvalbumin-immunoreactive structures in this nucleus. **C:** Calbindin immunoreactivity, note the moderate to high density of immunoreactive terminals, but lack of immunoreactive cells in this basal forebrain nucleus. **D:** Calretinin immunoreactivity, note the absence of calretinin-immunoreactive structures in this nucleus. In all images medial is to the left and dorsal to the top. Scale bar = 500 μm in D (applies to all); 100 μm in D inset (applies to all insets).

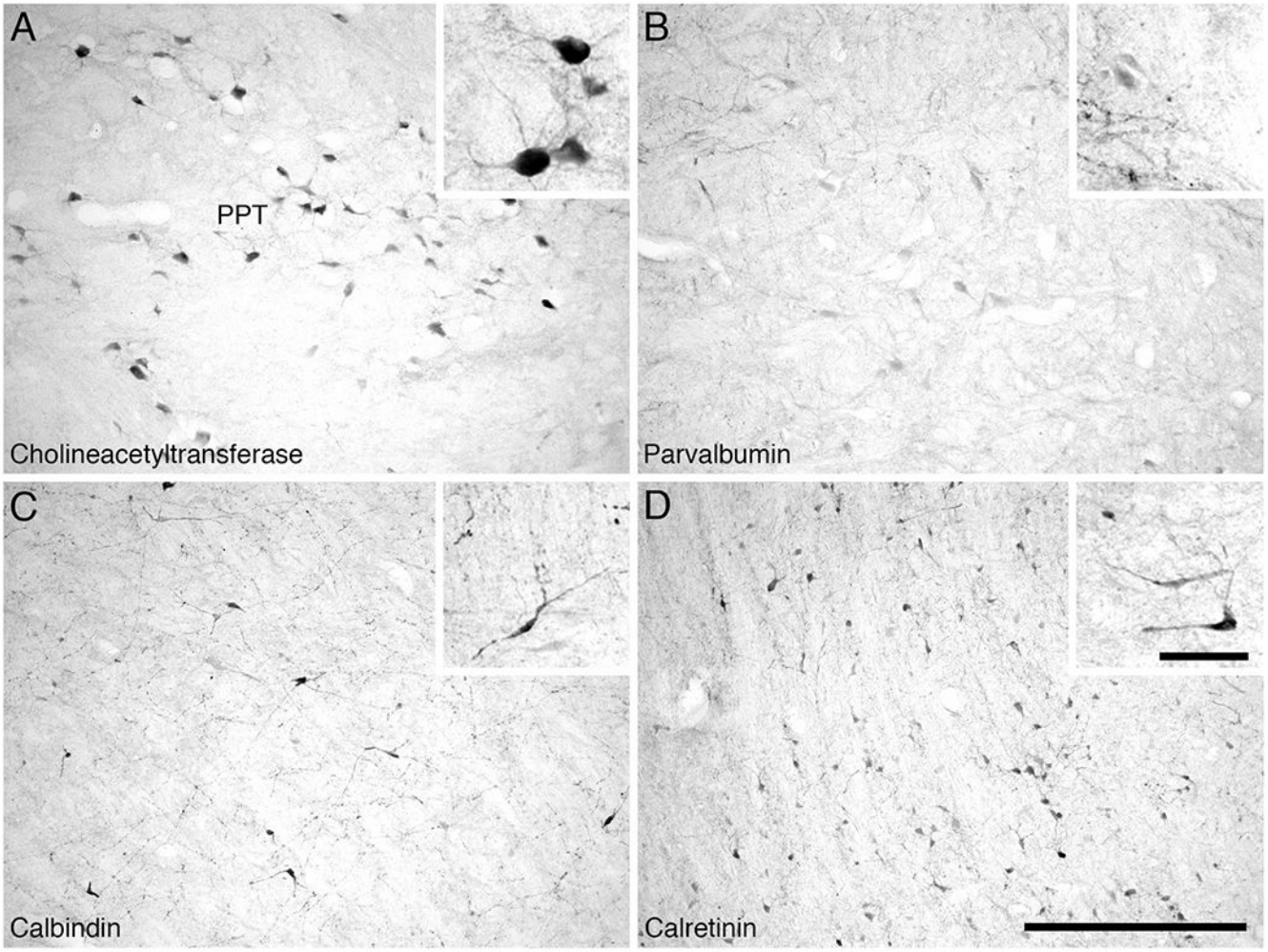

Figure 4.

Low (main image) and high (inset) magnification photomicrographs of the pedunculopontine tegmental cholinergic nucleus in the minke whale brain. **A:** Neurons immunoreactive for choline acetyltransferase showing part of the pedunculopontine tegmental nucleus (PPT). **B:** Parvalbumin immunoreactivity, note the low density of parvalbumin-immunoreactive structures in the PPT. **C:** Calbindin immunoreactivity, note the moderate and high density of cells and terminals, respectively, in the region of the PPT. **D:** Calretinin immunoreactivity, note the high density of cells and terminals in the PPT. In all images medial is to the left and dorsal to the top. Scale bar = 500 μm in D (applies to all); 100 μm in D inset (applies to all insets).

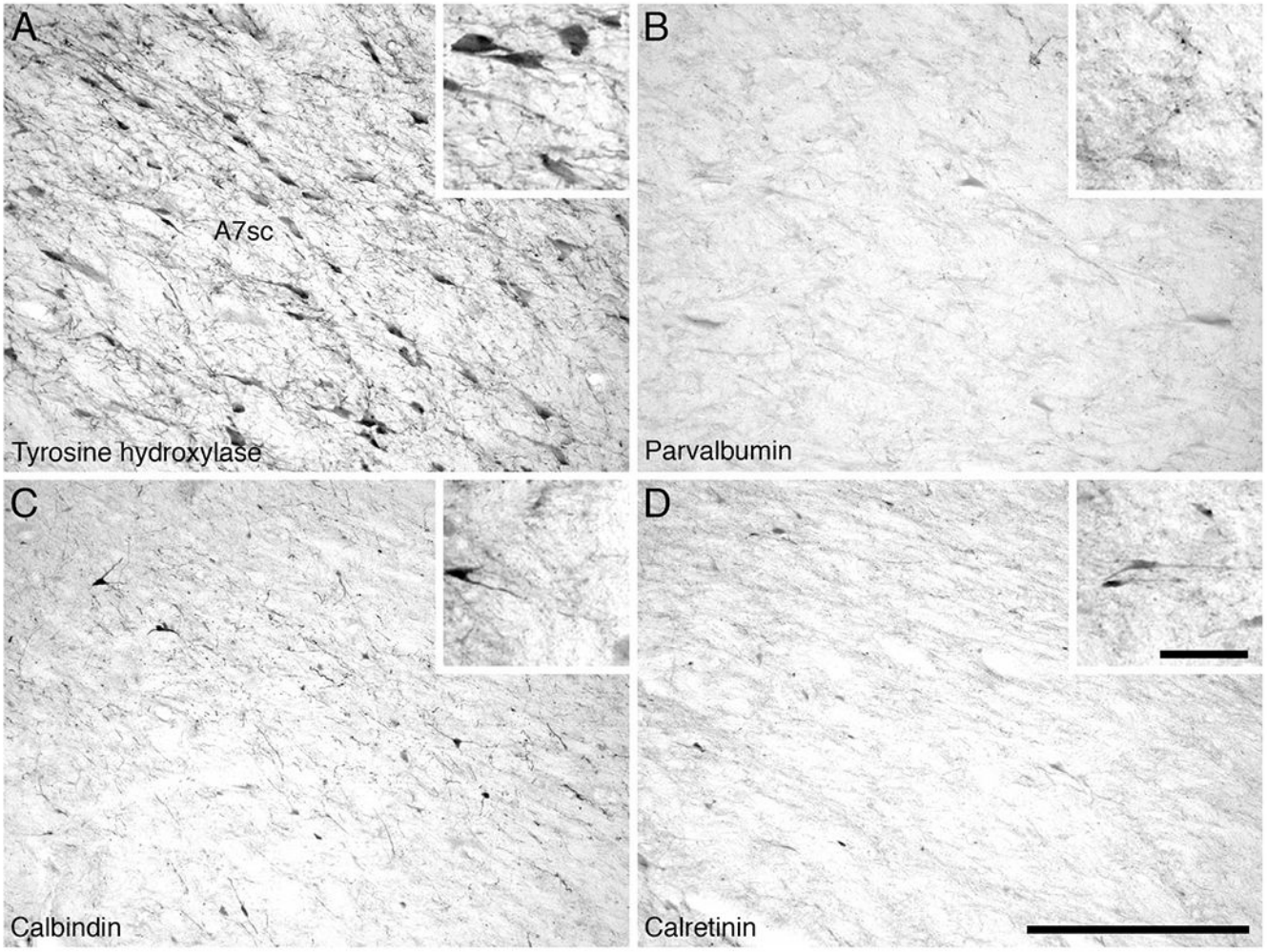

Figure 5.

Low (main image) and high (inset) magnification photomicrographs in the region of the subcoeruleus compact division (A7sc) of the locus coeruleus complex in the minke whale brain. **A:** Neurons immunoreactive for tyrosine hydroxylase showing the compact portion of the subcoeruleus (A7sc). Note the low density of parvalbumin (**B**), calbindin (**C**), and calretinin (**D**) immunoreactive structures in the A7sc of the minke whale. In all images medial is to the left and dorsal to the top. Scale bar = 500 μm in D (applies to all); 100 μm in D inset (applies to all insets).

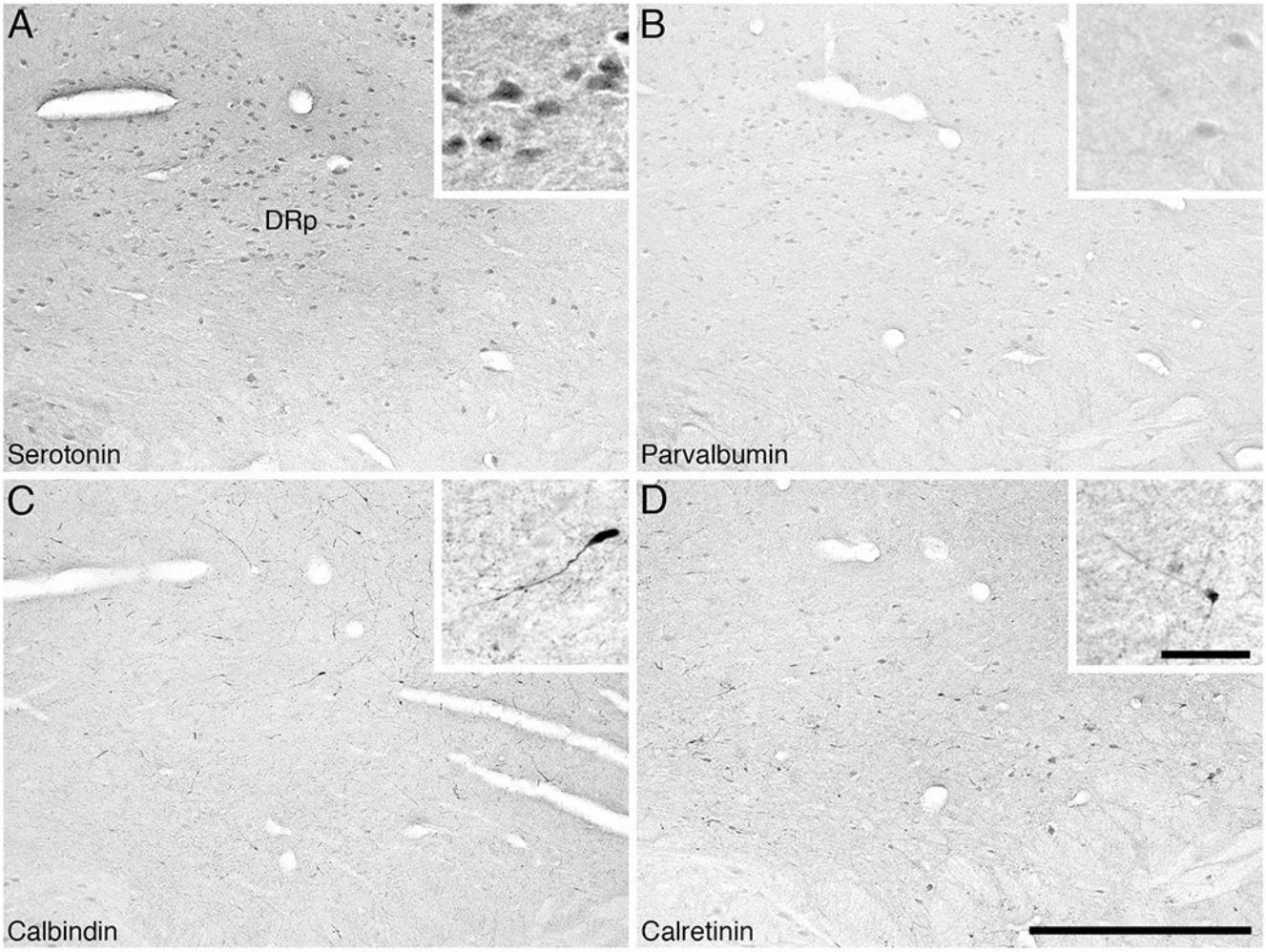

Figure 6.

Low (main image) and high (inset) magnification photomicrographs in the region of the dorsal raphe peripheral division (DRp) of the dorsal raphe nuclear complex in the minke whale brain. **A:** Neurons immunoreactive for serotonin showing the peripheral division of the dorsal raphe complex. **B:** Parvalbumin immunoreactivity, note the absence of parvalbumin immunoreactive structures in the DRp. **C:** Calbindin immunoreactivity, note the moderate density of cells and terminals. **D:** Calretinin immunoreactivity, note the moderate density of cells and terminals. In all images medial is to the left and dorsal to the top. Scale bar = 500 μm in D (applies to all); 100 μm in D inset (applies to all insets).

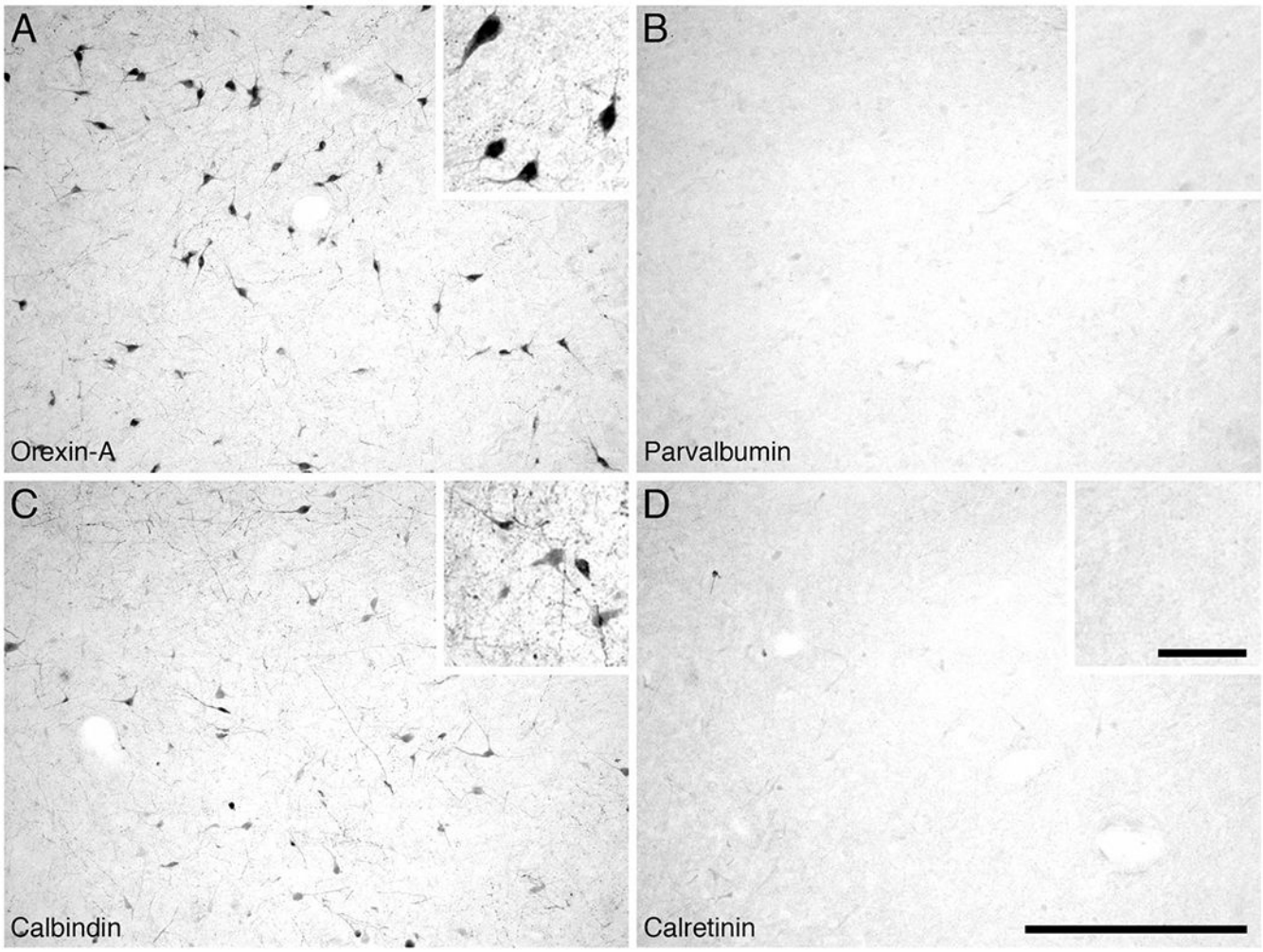

Figure 7.

Low (main image) and high (inset) magnification photomicrographs in the region of the main magnocellular orexinergic cluster in the hypothalamus of the minke whale. **A:** Neurons immunoreactive for orexin-A in the main cluster of the hypothalamus. **B:** Parvalbumin immunoreactivity, note the low density of parvalbumin immunoreactive structures in this hypothalamic region. **C:** Calbindin immunoreactivity, note the high and moderate density of cells and terminals, respectively, in this region of the hypothalamus. **D:** Calretinin immunoreactivity, note the low density of cells and moderate density of terminals in the main orexinergic cluster. In all images medial is to the left and dorsal to the top. Scale bar = 500 μm in D (applies to all); 100 μm in D inset (applies to all insets).

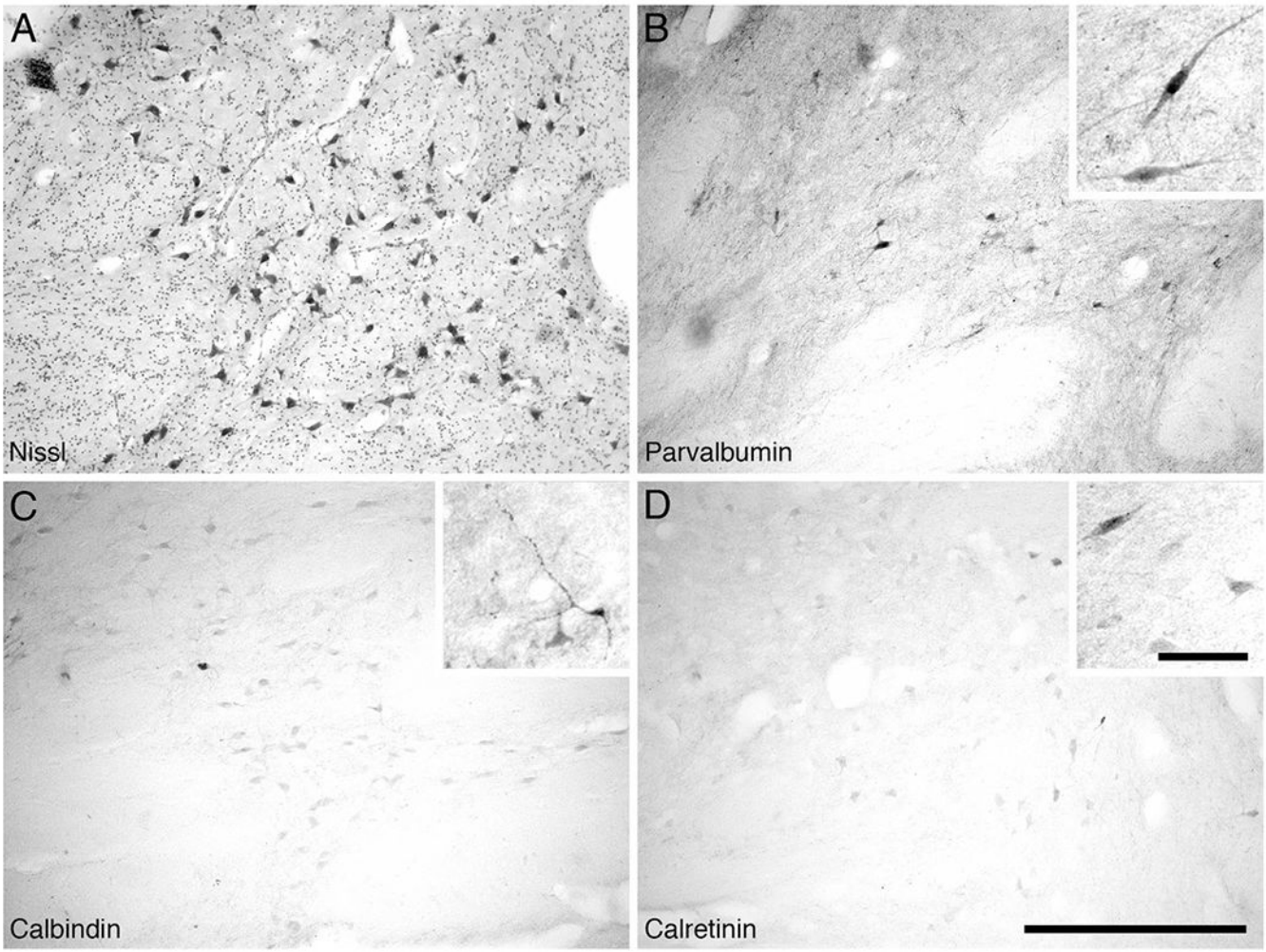

Figure 8.

Low (main image) and high (inset) magnification photomicrographs of the thalamic reticular nucleus in the diencephalon of the minke whale brain. **A:** Nissl stain showing the low density of neurons within the thalamic reticular nucleus. **B:** Parvalbumin immunoreactivity, note the moderate density of parvalbumin-immunoreactive cells and the high density of the parvalbumin-immunoreactive terminal network. A low to moderate density of calbindin (**C**) and calretinin (**D**)-immunopositive structures were observed. In all images medial is to the left and dorsal to the top. Scale bar = 500 μm in D (applies to all); 100 μm in D inset (applies to all insets).

TABLE 1.

Stereological Parameters Used for Estimating Neuron Numbers in the Minke Whale

Nucleus examined	Counting frame size (μm)	Sampling grid size (μm)	Disector height (μm)	Cut thickness (μm)	Average mounted thickness (μm)	Vertical guard zones (top and bottom, μm)	Section interval	Number of sections	Number of sampling sites	Average CE (Gundersen m = 0)	Average CE (Gundersen m = 1)
LDT (ChAT+)	200 × 200	200 × 200	15	50	30.9	5	20	19	2386	0.06	0.06
PPT (ChAT+)	200 × 200	800 × 800	15	50	35.8	5	20	19	485	0.09	0.08
LC (TH+)	150 × 150	800 × 800	15	50	34	5	20	15	421	0.14	0.11
Orexin (OxA+)	200 × 200	800 × 800	15	50	26.3	5	20	14	446	0.16	0.10

LDT=laterodorsal tegmental nucleus, PPT=pedunculopontine tegmental nucleus, LC=locus coeruleus complex, ChAT+=neurons immunopositive for cholineacetyltransferase, TH+=neurons immunopositive for tyrosine hydroxylase, OxA+=neurons immunopositive for orexin-A.

TABLE 2.

Stereological Results for Neuron Numbers, Volume, and Area in the Minke Whale

Nucleus examined	Total estimated population using mean section thickness	Average estimated cell volume (μm^3)	Average estimated cell area (μm^3)
LDT (ChAT+)	13,320	3011.55	1229.83
PPT (ChAT+)	260,922	3168.54	1227.13
LC (TH+)	203,686	1957.65	824.54
Orexin (OxA+) all cells	277,604	–	–
Orexin (OxA+) magnocellular	125,194	4719.90	2083.42
Orexin (OxA+) parvocellular	152,410	1790.43	864.69

LDT=laterodorsal tegmental nucleus, PPT=pedunculopontine tegmental nucleus, LC=locus coeruleus complex, ChAT+=neurons immunopositive for cholineacetyltransferase, TH+=neurons immunopositive for tyrosine hydroxylase, OxA+=neurons immunopositive for orexin-A.

TABLE 3.

Density of Neurons and Terminal Networks of the Calcium Binding Proteins Calbindin (CB), Calretinin (CR), and Parvalbumin (PV) in Relation to Various Sleep–Wake Nuclei in the Brain of the Minke Whale

	Calbindin		Calretinin		Parvalbumin	
Sleep-related nuclei	**Neurons**	**Terminal networks**	**Neurons**	**Terminal networks**	**Neurons**	**Terminal networks**
Cholinergic						
Diagonal band of Broca	+	+++	+	+	+	+
Islands of Calleja and olfactory tubercle	+++	+++	+	+	+	+
Nucleus basalis	+++	+++	++	++	++	+
Pedunculopontine tegmental nucleus	++	+++	+++	+++	+	+
Laterodorsal tegmental nucleus	++	+++	++	++	+	++
Catecholaminergic						
Compact subcoeruleus (A7sc)	+	++	+	+	+	++
Diffuse subcoeruleus (A7d)	+	+	++	++	−	+
Diffuse locus coeruleus (A6d)	++	+++	++	+++	+	++
Serotonergic						
Dorsal raphe, interfascicular (DRif)	+	++	++	++	−	−
Dorsal raphe, ventral (DRv)	++	+	++	++	+	+
Dorsal raphe, dorsal (DRd)	++	+++	++	++	+	+
Dorsal raphe, lateral (DRl)	++	+++	+++	+++	+	+
Dorsal raphe, peripheral (DRp)	+++	+++	++	+++	+	+
Dorsal raphe, caudal (DRc)	++	+++	++	+++	−	+
Orexinergic						
Main cluster	+++	++	+	++	+	+
Optic tract cluster	++	++	+++	+++	+	++
Zona incerta cluster	+++	++	+++	++	−	−
Parvocellular cluster	++	+++	+++	+++	−	+
Thalamic reticular nucleus	+	+	+	++	++	+++